Cooperativity among defect sites in AO_{2+x} and A_4O_9 (A=U,Np,Pu): Density functional calculations

D. A. Andersson,[1] J. Lezama,[1,2] B. P. Uberuaga,[1] C. Deo,[3] and S. D. Conradson[1]
[1]*Materials Science and Technology Division, Los Alamos National Laboratory, Los Alamos, New Mexico 87545, USA*
[2]*Departamento de Fisica Aplicada, CINVESTAV-Merida, Merida Yucatan Mexico, 97310*
[3]*Nuclear and Radiological Engineering Program, George W. Woodruff School of Mechanical Engineering, Georgia Institute of Technology, Atlanta, Georgia 30332, USA*
(Received 18 October 2008; published 28 January 2009)

Actinide dioxides derived from the AO_2 fluorite lattice are of high technological relevance due to their application in nuclear reactor fuels. In this paper we use density functional theory calculations to study the oxidation of uranium, neptunium and plutonium dioxides, AO_2 (A=U, Np, or Pu), in O_2 and O_2/H_2O environments. We pay particular attention to the formation of oxygen clusters (cooperativity) in AO_{2+x} and how this phenomenon governs oxidation thermodynamics and the development of ordered A_4O_9 compounds. The so-called split di-interstitial, composed of two nearest-neighbor octahedral oxygen interstitials that dislocate one regular fluorite lattice oxygen ion to form a cluster of triangular geometry, is predicted to be the fundamental building block of the most stable cluster configurations. We also identify how the formation of oxygen defect clusters and the degree of oxidation in AO_{2+x} are both governed by the ability of the O $2p$ orbitals of the interstitial-like ($+x$) ions to hybridize with regular fluorite lattice ions.

DOI: 10.1103/PhysRevB.79.024110 PACS number(s): 61.72.J−

I. INTRODUCTION

The technological importance of actinide dioxides, AO_2 (A=U, Np or Pu), largely originates from their application in nuclear reactor fuels. Today many reactors use UO_2 as the primary fuel component. While low-burn up spent fuels contain large amounts of radioactive materials, in order to reduce the amount of waste requiring long-term storage, there are on-going efforts to develop fast reactors capable of utilizing a larger fraction of the fuel for energy production. This approach calls for complex multicomponent fuels that, in addition to the UO_2 matrix, contain significant amounts of transuranic elements (Np, Pu, etc.). Oxidation of AO_2 compounds emerges as a central theme in fuel fabrication, reactor operation, long-term storage forms for both spent fuels and surplus weapons materials, and environmental actinide migration.

The reduction-oxidation properties of AO_2 demonstrate significant variability along the actinide series, e.g., while UO_2 easily reacts with oxygen,[1–3] PuO_2 and later actinide oxides are less prone to oxidation.[1,4,5] PuO_2 seems to require special conditions in order to accommodate excess oxygen.[4,6–8] These complexities are all related to the unique behavior of the A $5f$ electrons and the unusually high degree of covalent mixing or hybridization in chemical bonds between oxygen and actinides. Upon oxidation UO_{2+x} retains the parent fluorite structure up to the terminal U_4O_9 compound, which exhibits an ordered arrangement of interstitial-like oxygen ions within the fluorite lattice.[9,10] PuO_2 was long thought to be the highest stable oxide of plutonium,[1,5] however Haschke and co-workers[6,7] found that PuO_2 reacts with moist air to form PuO_{2+x} with $x \leq 0.27$. Subsequent EXAFS studies by Conradson and co-workers[11,12] demonstrated that PuO_{2+x} compounds are more accurately represented as $PuO_{2+x-2y}(OH)y \cdot z(H_2O)$ due to the affinity to H_2O and/or OH^- species. No ordered Pu_4O_9 compound has been identified.[7] NpO_{2+x} compounds that are derived from the NpO_2 fluorite lattice have not been reported in the literature and the experimental phase diagram points to a two-phase-field that involves NpO_2 and Np_2O_5 below $\approx$700 K.[13,14] Even though the NpO_{2+x} fluorite phase is metastable with respect to $NpO_2+Np_2O_5$ (Refs. 13 and 14) or NpO_2+O_2,[4,13,14] its properties are important for multicomponent $(U,Np,Pu,\ldots)O_{2+x}$ materials since the hyperstoichiometric fluorite phase should be stabilized in uranium containing solid solutions, $(U,Np)O_{2+x}$.

Theoretical studies of actinide dioxides predict oxidation of UO_2 to be exothermic[15–20] while oxidation of PuO_2 is predicted to be endothermic.[16,21,22] These studies are complicated by the strongly correlated nature of A $5f$ electrons, which cause conventional exchange-correlation functionals, e.g., the local-density approximation (LDA), to describe actinide dioxides as ferromagnetic metals instead of antiferromagnetic Mott insulators. There are, however, promising approaches to address this issue, such as the LDA+U method,[18–20,23–27] hybrid density functionals,[21,28–30] the self-interaction corrected methodology (SIC) (Ref. 22) and dynamical mean field theory (DMFT).[31] In addition to the delicate electronic properties of AO_{2+x}, the interstitial-like excess oxygen ions exhibit complex structural properties that include cluster formation (cooperativity) and strong interaction with the host fluorite lattice.[9–12,32–36] With exception for the recent publication by Geng *et al.*,[37] existing theoretical studies predominantly rely on simplistic structure models of AO_{2+x} and/or A_4O_9 that essentially ignore clustering effects.[15–22]

The present paper is motivated by the persisting incomplete experimental and theoretical understanding of actinide dioxides, in particular for issues regarding oxygen clustering phenomena and their relation to the thermodynamic and kinetic properties of AO_{2+x}. We investigate the oxidation of UO_2, NpO_2, and PuO_2 by applying density functional theory

TABLE I. Calculated lattice parameters (a_0) and bulk moduli (B_0) of AO_2 (A=U, Np or Pu) compounds. Experimental reference values are shown within parenthesis.

	UO_2	NpO_2	PuO_2
a_0(Å)	5.448(5.47[a])	5.398(5.43[a])	5.354(5.394[b])
B_0(GPa)	218 (207[c,d])	228 (200[c,d])	226 (178[d])

[a]Reference 44.
[b]Reference 6.
[c]Reference 45.
[d]Reference 46.

(DFT) calculations to study the structure, thermodynamic stability, and electronic characteristics of interstitial oxygen clusters in AO_{2+x} and how these clusters may order in the terminal A_4O_9 compounds. The role of H_2O and hydrolysis products (OH^-) in the oxidation process is also addressed.

Our paper is organized as follows. Section II describes details of the theoretical methodology to be used. Section III A provides a brief overview of existing structure models for the UO_{2+x} system and explains the fundamental aspects of their electronic structure. Section III B presents new concepts and results for the geometry and stability of defect clusters in AO_{2+x}. The corresponding ordering patterns in the terminal A_4O_9 compounds are explored in Sec. III C. We also analyze the particular features of the A $5f$ electronic structure that drive clustering (cooperativity) in AO_{2+x}/A_4O_9 compounds and formulate a common framework for UO_{2+x}, NpO_{2+x} and PuO_{2+x}.

II. METHODOLOGY

The DFT calculations were performed with the Vienna *Ab Initio* Simulation Package (VASP) (Refs. 38–40) using the projector augmented wave (PAW) method.[41,42] The rotationally invariant LDA+U functional due to Lichtenstein *et al.*[43] was employed to describe the exchange and correlation effects. This method applies the local-density approximation (LDA) together with an Hubbard U term that improves handling of the intraband Coulomb repulsion among the $5f$ electrons. Unlike conventional LDA or generalized gradient approximation (GGA), the LDA+U functional captures the Mott insulating properties of the strongly correlated U $5f$, Np $5f$, and Pu $5f$ electrons in AO_2 adequately. The LDA+U approach contains two *a priori* unknown parameters; the spherically averaged screened Coulomb energy, U, and the exchange energy, J. For UO_2, U and J parameters of 4.5 and 0.51 eV, respectively, were originally derived by Dudarev *et al.*[23] and have since been widely applied.[18–20,37] Here we adopt these parameters. We applied U=4.0 eV and J =0.7 eV for the Pu $5f$ orbitals, which is within the parameter range specified in the literature.[24,25] The U and J parameters for the Np $5f$ orbitals were set to 4.25 eV and 0.6 eV, which represent an average between the U $5f$ and Pu $5f$ values. This choice accounts rather accurately for the experimental lattice parameter and bulk modulus of NpO_2 (see Table I). The occupied Np $5f$ orbitals are predicted to form a narrow band right at the top of the valence O $2p$ band, which is similar to the band structure obtained from parameter-free hybrid functionals,[28] though the latter predicts a tiny gap between the O $2p$ band and the Np $5f$ peak. Spin polarization was applied for all AO_{2+x} compounds and, unless otherwise stated, antiferromagnetic spin alignment was used. This configuration was obtained as the ground-state for UO_2 and PuO_2, while NpO_2 preferred ferromagnetic ordering by 0.004 eV. Spin-orbit coupling was not considered, since, even though spin-orbit coupling will change the details of the magnetic ground state by splitting the f orbitals, this effect is believed to have limited influence on the thermodynamic and structural properties of current interest.[30] The LDA+U lattice constant and bulk modulus predictions for the AO_2 compounds are summarized in Table I, together with experimental estimates. The calculated lattice parameters agree well with experiments and, even though there are some discrepancies for the bulk moduli, the calculated values are considered to be reasonable, particularly in view of known uncertainties for the experimental PuO_2 bulk modulus.[24] A $2\times2\times2$ supercell expansion of the cubic fluorite unit cell was used to study defect properties. The volume of the supercell was fixed at the calculated volume of UO_2, NpO_2, and PuO_2, respectively. All defect calculations used a $2\times2\times2$ Monkhorst-Pack k-point mesh[47] with a Gaussian smearing of 0.05 eV. The plane-wave cut off was set to 400 eV. All internal structural parameters were relaxed until the total energy and the Hellmann-Feynman forces on each ion were $<$0.02 eV/Å. As discussed in Sec. III C, a number of ordered A_4O_9 compounds have been studied. The unit cells of these structures are spanned by two different sets of vectors; [1 1 0],[0 1 1],[1 0 1] and [2 2 0],[0 0 1],[0.5 –0.5 0], which are defined with respect to the conventional cubic fluorite unit cell. For the first cell we applied a $2\times2\times2$ Monkhorst-Pack k-point mesh and for the second cell we applied a $2\times4\times6$ mesh. Volume relaxation was taken into account for both cells. In order to assess the oxidation thermodynamics in O_2 and H_2O chemical environments (gaseous form is assumed throughout this work), reference energies for these molecules (chemical potentials) must be established. These energies were calculated by placing an isolated molecule inside a large supercell and relaxing the geometry. Since DFT within the LDA formulation is known to overestimate the binding energy of many molecules, we have applied correction terms of 2.4 eV (Ref. 48 and 49) and 1.5 eV (Ref. 48) for O_2 and H_2O molecules, respectively. The oxidation energy of AO_{2+x} is defined as the energy associated with the $\frac{1}{x}AO_2+\frac{1}{2}O_2\rightarrow\frac{1}{x}AO_{2+x}$ reaction or, when appropriate, the corresponding reaction that includes H_2O. Negative oxidation energies imply spontaneous oxidation and positive numbers are equivalent to instability of the hyperstoichiometric compounds.

AO_{2+x} compounds contain a distribution of A^{5+} ions as charge-compensating defects and there are two A^{5+} ions for each excess oxygen ion. The total energy of AO_{2+x} compounds depends, not only on the distribution of excess O^{2-} ions, but also on the distribution of A^{5+} ions, as identified by orbital projected spin densities, with respect to the position of the excess ions. In addition to the ground-state structures, it is possible to obtain metastable A^{5+} distributions from the DFT calculations. All numbers that are reported here refer to

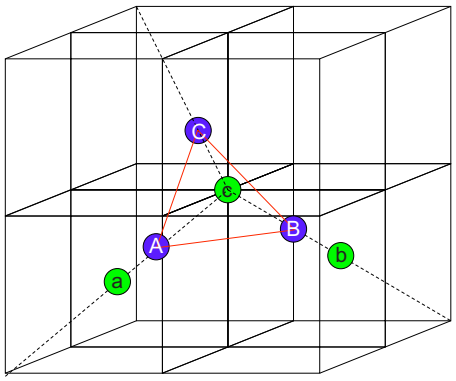

FIG. 1. (Color online) Idealized schematics of the structure of the undistorted (I_2^O, lower case letters) and split (I_2^X, upper case letters) di-interstitial structures. The cubes represent the simple-cubic oxygen sublattice; for clarity, uranium ions are not shown. The I_2^O structure has two oxygen interstitials (*a* and *b*) in octahedral-interstitial sites in the lattice. The I_2^X structure constitutes an equiaxed or equilateral triangle that is situated on top of an empty fluorite lattice oxygen site.

the lowest energy solution that we are able to attain for each structure.

III. RESULTS AND DISCUSSION

A. Existing interstitial clustering models and analysis of their electronic structure

1. Uranium dioxide

The AO_2 fluorite lattice has large empty octahedral sites that appear to be the natural location for excess oxygen ions. Willis and co-workers[34,35] found that in UO_{2+x} such interstitials tend to aggregate into clusters composed of multiple interstitial ions interacting with regular oxygen ions to form complex defect clusters.[33–36] They initially proposed the so-called 2:2:2 cluster, which is effectively composed of two oxygen vacancies and four interstitials (see for example Fig. 3 in Ref. 33). Bevan *et al.*[9] revised the UO_{2+x} structure model and suggested that the excess oxygen ions occupy the cubo-octahedral holes of the fluorite lattice. In this model each defect cluster contains 12 ions, of which four are ascribed as excess oxygen ions and the remaining eight ions are displaced from their fluorite lattice positions (see for example Fig. 2 in Ref. 9). The best agreement with experiments is achieved when the octahedral-interstitial hole enclosed by the cubo-octahedron cluster is also occupied.[10] EXAFS measurements by Conradson *et al.*[32] have further illustrated the complexity of UO_{2+x} by suggesting a U-O coordination that includes 1.74 Å bonds.

Ichinomiya *et al.*[50] and Govers *et al.*[51] used empirical potentials to investigate the stability of di-interstitial clusters in UO_{2+x} and, in contrast to experiments, they found the 2:2:2 cluster to be metastable, or even unstable. In its place they predicted the stable di-interstitial oxygen cluster to be composed of three oxygen ions arranged in an equiaxed or equilateral triangle that is situated in a {111} plane above an empty regular oxygen site (see Fig. 1). Andersson *et al.*[52]

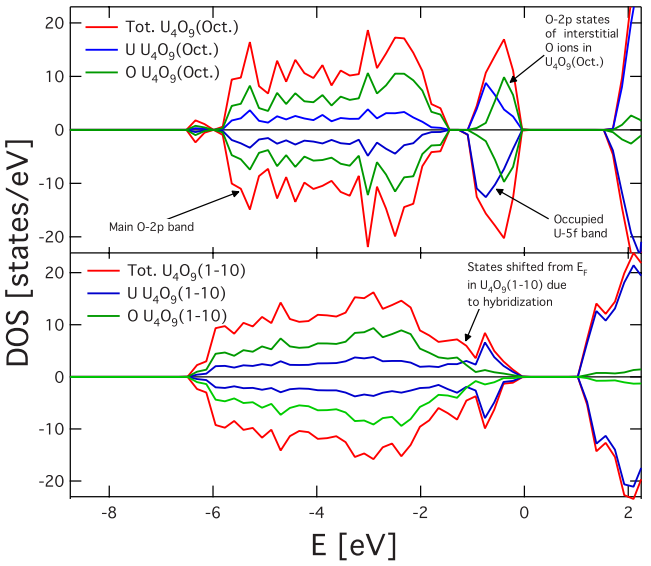

FIG. 2. (Color online) Density of states (DOS) and projected density of states (PDOS) for U_4O_9 constructed from an ordered arrangement of split di-interstitials, $U_4O_9(1-10)$, and from octahedral interstitials, U_4O_9(Oct.). Notice that the U $5f-$O $2p$ gap remains for the octahedral-interstitial structure, while for the split di-interstitial structure the O $2p$ states overlapping with U $5f$ peak in the octahedral structure moves down to overlap with the main O $2p$ band. The highest occupied state is at 0 eV.

confirmed these conclusions using DFT calculations and they labeled this defect as split di-interstitial, I_2^X. Here the "*I*" denotes an interstitial type of defect, the subscript 2 denotes the number of interstitials that are involved and the superscript "*X*" denotes their particular geometric configuration. This notation is used throughout this paper to designate different types of excess oxygen defects. The split di-interstitial is created from two nearest-neighbor interstitial ions (*a* and *b* in Fig. 1) that move toward a common regular oxygen site, dislocating it (*c* in Fig. 1), thus creating the split di-interstitial and the vacant site that serves as its center of mass (*A*, *B*, and *C* in Fig. 1).

Adding oxygen to UO_2 results in charge transfer from the $5f$ orbitals of U^{4+} ions to the $2p$ orbitals of the excess oxygen ions. The high stability of split di-interstitals in UO_{2+x} can be explained by the fact that this structure allows the orbitals occupied by the transferred electrons to hybridize with the uranium orbitals and thus imitate the uranium-oxygen interaction in the ideal fluorite lattice, in particular the covalent contribution to the uranium-oxygen bonding. This process enables the excess O $2p$ orbitals to move down from the U $5f$ states at the Fermi level to the main O $2p$ band, thus decreasing the band energy and, unless the corresponding increase in electrostatic energy among ions dominates, also the total energy (illustrated for U_4O_9 in Fig. 2). As a consequence, the O $2p-$U $5f$ gap found in UO_2 diminishes or even disappears. Oxygen ions in octahedral-interstitial sites are unable to interact with the uranium ions as efficiently as split di-interstitials or regular fluorite oxygen ions and, consequently, the excess O $2p$ orbitals for octahedral interstitials cannot merge with the main O $2p$ band. For this reason they do not experience the same gain in band energy

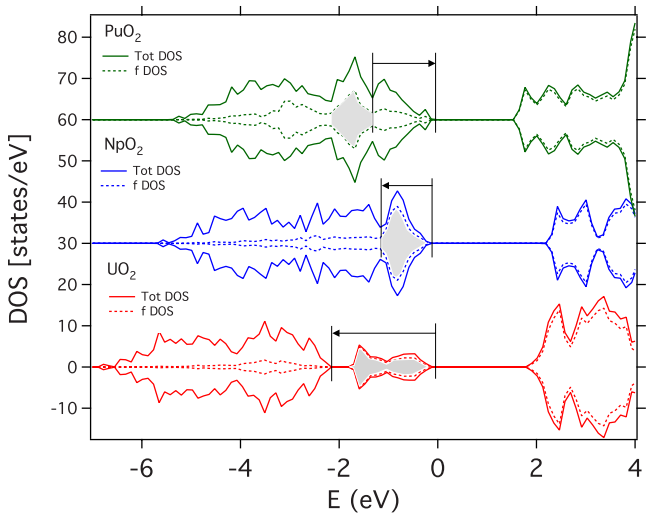

FIG. 3. (Color online) The density of states for UO_2, NpO_2, and PuO_2. The NpO_2 and PuO_2 DOS have been shifted from the zero line. The position of the *A* 5*f* bands is shown in dashed lines, including both localized states (shaded in gray) and states hybridized with the O 2*p* band. The arrows indicate the separation of the localized *A* 5*f* states and the O 2*p* bands. The highest occupied state is at 0 eV.

as split di-interstitials. However, due to the larger separation of excess O^{2-} ions and of charge compensating U^{5+}/U^{6+} ions, octahedral interstitials are more favorable from the perspective of Coulomb repulsion among ions. Qualitatively, this implies that the defect stability in UO_{2+x} is a competition between hybridization (decrease of the band energy) and Coulomb repulsion among ions. The former favors the split di-interstital type of structures while the latter favors structures based on isolated octahedral interstitals. Figure 2 illustrates the band structures of two U_4O_9 compounds; one based on octahedral interstitials and another one composed of ordered split di-interstials. We pay particular attention to the highlighted difference in the band-structure position of the excess O 2*p* orbitals, and thus hybridization, between these two structures.

Let us take a closer look at the underlying mechanisms for the hybridization features discussed in the previous paragraph. The projected DOS for UO_2 (partially illustrated in Fig. 3) reveals that there is a sizable U 5*f*/U 6*d* contribution in the main O 2*p* band.[28] At the same time, an electron count shows that all the U 5*f* electrons that are expected from the formal valence of the U^{4+} ions (two) are located in the U 5*f* peak above the edge of the main O 2*p* band. This implies that the U 5*f*/U 6*d* contribution in the O 2*p* band originates from overlap or hybridization of nominally filled O 2*p* orbitals with nominally empty U 5*f*/U 6*d* orbitals. This UO_2 hybridization is not available for the octahedral-interstitial oxygen ions in U_4O_9(Oct.) since their interaction with the uranium ions is shielded by the cubic cage of regular fluorite oxygen ions. Instead the nearest-neighbor uranium interaction for the octahedral oxygen interstitials is such that their O 2*p* orbitals almost overlap with the U 5*f* states in the band gap, as indicated by Fig. 2. The split di-interstitial U_4O_9 structures, on the other hand, allow the O 2*p* orbitals of both the regular fluorite oxygen ions and the excess ions to overlap or hybridize with the nominally empty U 5*f*/U 6*d* orbitals, which, as mentioned above, facilitates for the excess O 2*p* orbitals to move down from the U 5*f* states at the Fermi level to the main O 2*p* band (Fig. 2) and thus decrease the band energy. We conclude that the overlap of excess O 2*p* orbitals with the main O 2*p* band is in fact driven by the hybridization of excess O 2*p* orbitals with nominally empty U 5*f*/U 6*d* orbitals made possible by the particular structural distortion for split di-interstitials. Figure 2 also reveals that the calculations predict the band gap (valence to conduction band) to decrease by $\approx$0.45 eV for structures built from split di-interstitials [U_4O_9(1–10) in this particular case], as compared to octahedral interstitials, and by $\approx$0.70 eV compared to UO_2. This is an indicator of the changes in O 2*p*–U 5*f*/U 6*d* hybridization that takes place for split di-interstitial structures.

2. Neptunium and plutonium dioxides

Band-structure calculations reveal that the 5*f* electrons in UO_2 are situated $\approx$0.6 eV above the O 2*p* valence-band edge, while the corresponding Np 5*f* states are right at the top of the O 2*p* band. For PuO_2 the 5*f* states overlap with the O 2*p* band and together they form a more or less continuous band. Due to the shift in position of the occupied 5*f* orbitals, the gain in band energy coming from charge transfer and hybridization between neptunium ions and the excess oxygen ions should be smaller than for UO_{2+x}. Another way of stating this would be that the difference between the delocalization energy of Np 5*f* electrons ($Np^{4+} \rightarrow Np^{5+}$) and the energy of these electrons occupying the (hybridized) O 2*p* band decreases compared to UO_2. This effect is even stronger for PuO_{2+x} and, in fact, the Pu^{4+} to excess oxygen charge transfer may result in increasing band energy. Figure 3 highlights the change in band structure between UO_2, NpO_2, and PuO_2. We note that the shift in the separation of the O 2*p* and *A* 5*f* bands is a qualitative measure of the ease of oxidation; large positive separation (long arrow pointed to the left in Fig. 3) implies negative oxidation energy and as the *A* 5*f* states move down below the main O 2*p* band-edge oxidation becomes more difficult (shorter "left" arrow and arrow pointed to the right in Fig. 3). Qualitatively, upon oxidation the *A* 5*f* electrons move to the top of the O 2*p* band and, consequently, the relative *A* 5*f*/O 2*p* position is closely related to the oxidation thermodynamics, via the band energy. We remark that for UO_{2+x} this picture corresponds to maximum gain in band energy and, as we have seen in Fig. 2, the real band structure for UO_{2+x} is somewhat more complicated but, at least qualitatively, the concept presented above is still valid. An immediate consequence of this band-structure effect is that the excess oxygen ions in PuO_{2+x} exhibits a different valence state than for UO_{2+x}. Analyses of spin densities reveal that excess oxygen ions in UO_{2+x} act as O^{2-}, while the corresponding state for PuO_{2+x} is $O^{(2-\delta)-}$, where $0<\delta<0.5$ and the exact δ value is structure dependent. δ values close to 0 correspond to split di-interstitial structures and the higher values to structures based on regular octahedral interstitials, i.e., the higher degree of hybridization for split di-interstitials facilitates higher valence but compared to

TABLE II. The oxidation energy for various defects in AO_{2+x}, differently ordered A_4O_9 compounds and hydrogen-containing AO_{2+x}/A_4O_9 compounds. The UO_{2+x} data are partially reproduced from Ref. 52. The type of defect and defect ordering is indicated within parenthesis, e.g., $A_{32}O_{65}(I_1)$ for one single interstitial in the $2\times2\times2$ supercell. See text for labeling. The values within parenthesis for Pu_4O_9(Oct.) and Np_4O_9(Oct.) correspond to an octahedral-interstitial compound that contains O_2 species (see text). All energies are in eV and measured per excess oxygen ion. For the small unit cells, the values within brackets represent the change in lattice parameter (in Å) compared to AO_2 (volume relaxation was not performed for the cases where this number is missing). N/A designates that this particular compound was not studied.

	$A_{32}O_{65}(I_1)$	$A_{32}O_{66}(I_2^0)$	$A_{32}O_{66}(I_2^S)$	$A_{32}O_{66}(I_2^X)$	$A_{32}O_{68}(I_4^X)$	$A_{32}O_{68}(I_4^S)$
UO_2	−2.53	−2.21	−2.38	−2.34	−2.71	−2.32
NpO_2	−0.32	−1.29	−0.16	−0.34	−0.71	−0.18
PuO_2	0.44	0.50	0.13	0.45	−0.12	0.04
	$A_{32}O_{68}(I_4^C)$	$A_{32}O_{69}(I_5^C)$	A_4O_9(Oct.)	$A_4O_9(111_0)$	$A_4O_9(111)$	$A_4O_9(1-10)$
UO_2	−2.25	−2.50	−1.86[−0.05 Å]	−2.05[−0.03 Å]	−2.11[−0.01 Å]	−2.25[−0.02 Å]
NpO_2	N/A	N/A	0.39(−0.37)[0.01 Å]	−0.18[−0.01 Å]	−0.22[−0.01 Å]	−0.56[−0.01 Å]
PuO_2	N/A	N/A	0.34(−0.13)[0.03 Å]	0.00[0.02 Å]	0.14[0.01 Å]	0.46[−0.01 Å]
	A_4O_9(bcc)	A_4O_9(bccr)	A_4O_9(Cubo)	$AO_2(H_2O)_{1/32}$	$AO_2(OH)_{1/32}$	$A_4O_8(OH)_2$
UO_2	−2.63	−2.62	−2.13	N/A	−2.11	−1.81[0.03 Å]
NpO_2	−0.86	−0.83	N/A	N/A	−0.55	−0.69[0.03 Å]
PuO_2	−0.14	−0.09	N/A	0.47	0.09	−0.60[0.03 Å]

UO_{2+x} this process is still incomplete. The charge-compensating plutonium ions also deviate from the pentavalent state of U^{5+} ions and exhibit partially reduced valency. All together this indicates that complete charge transfer between localized Pu $5f$ and excess O $2p$ orbitals is not favorable. Here, charge transfer refers to delocalizing one electron from the $5f$ orbitals and allowing it to participate in A-O bonding, which, as discussed above, includes both direct charge transfer and hybridization. The valence states in NpO_{2+x} suggest that it should be classified in the same category as PuO_{2+x}, but with smaller δ values, which is consistent with the occupied Np $5f$ states being situated at the top of the O $2p$ band and thus in between the position of the occupied U $5f$ and Pu $5f$ orbitals. The fact that charge transfer is incomplete in PuO_{2+x} and NpO_{2+x} creates unfilled states in the O $2p$ valence band, which, from a chemical point of view, is unfavorable and, as discussed in Secs. III C and III D, this has important consequences for the oxidation thermodynamics. Following the trends for the position of the $5f$ electrons along the actinide series we expect that actinide dioxides to the left of UO_2 (PaO_2) should oxidize easily, while actinide oxides to the right of PuO_2 should be very hard to oxidize.

The band-structure concepts presented above will be used as basis for the forthcoming discussion of AO_{2+x}/A_4O_9 structures and their thermodynamic stability.

B. New geometries and stabilities of oxygen clusters in AO_{2+x}

1. Uranium dioxide

Table II summarizes the oxidation energies (stabilities) of di-interstitial defect clusters in UO_{2+x}, NpO_{2+x}, and PuO_{2+x}. For now we focus on mono- and di-interstitials, I_1 and I_2, in UO_{2+x} and ignore other data in Table II. Andersson *et al.*[52] showed that in the low-concentration regime the split di-interstitials are essentially degenerate with two isolated interstitials (I_2^S), the latter being somewhat lower in energy. These two defects constitute the most stable configurations of two excess oxygen ions within the $2\times2\times2$ supercell and most notably undistorted, but still relaxed, di-interstitials (I_2^0), i.e., two nearest-neighbor interstitials without the accompanying dislocation of any regular oxygen ions, are predicted to be higher in energy than split di-interstitials. The oxidation energy of a single isolated oxygen interstitial in the $2\times2\times2$ supercell (I_1) is still lower than for either I_2^X or I_2^S, which means that in the dilute limit the binding energy for any di-interstitial cluster is negative and they should thus dissolve. This energy balance is an effect of the aforementioned competition between Coulomb repulsion among ions and hybridization.

The cubo-octahedron cluster (I_4^C) proposed for UO_{2+x} (Refs. 9 and 10) contains four excess oxygen ions and thus represents a larger and more extended defect than the di-interstitial type of clusters. In order to evaluate its stability we have studied a single cubo-octahedral cluster embedded in the $2\times2\times2$ supercell and, similarly, we have also studied the cubo-octahedron structure with the central octahedral hole occupied by another excess oxygen ion (I_5^C), giving a cluster composed of five excess oxygen ions. For comparison, we have also treated clusters composed of two split di-interstitials, hereby denoted split quadinterstitial (I_4^X), as well as four octahedral interstitials homogeneously distributed within the $2\times2\times2$ supercell (I_4^S). The geometry of the most stable split quadinterstitial configuration is such that the two split di-interstitials are aligned along the [0.5 0 0] lattice

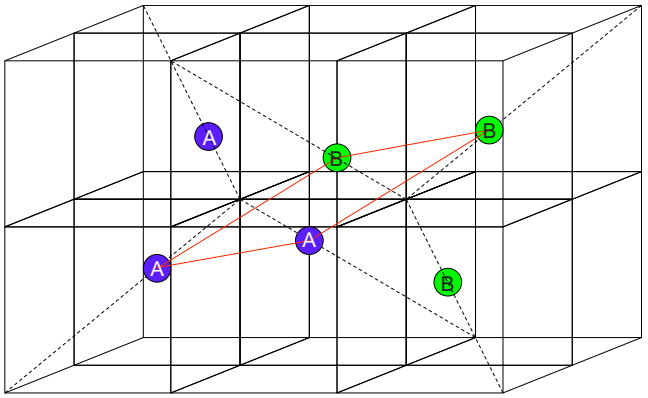

FIG. 4. (Color online) Idealized schematics of the split quadinterstitial (I_4^X). The cubes represent the simple-cubic oxygen sublattice; for clarity, uranium ions are not shown. The dashed lines indicate the particular cube diagonals, along which the interstitial and regular oxygen ions that belong to the defect cluster are displaced. The two split di-interstitials that make up the quadinterstitial are highlighted by A and B, respectively. The parallellogram formed by the adjoining base lines of the two split di-interstitials is outlined.

vector and rotated 180° with respect to each other (see Fig. 4). The stabilities (oxidation energies) of these structures are collected in Table II (labeled as I_4 and I_5). The split quadinterstitial cluster is the most stable configuration, followed by the cubo-octahedron cluster with occupied octahedral hole (I_5^C) and both of them are more stable than the structure based on regular octahedral interstitials. The simple cubo-octahedron (I_4^C) is significantly less stable than the I_5^C structure, which agrees with the findings by Geng *et al.*[37] Moreover, we confirm the observation that the central octahedral oxygen ion in the I_5^C cluster is rather significantly displaced from its ideal position.[37] The addition of an excess oxygen ion to the center of the cubo-octahedron cluster creates a structure that in many aspects resembles the split quadinterstitial structure, in particular after the displacement of the central ion from the high-symmetry position. The key electronic structure difference between the split quad- and octahedral-interstitial structures is that the former enables efficient O $2p$ hybridization for the excess ions and thus lowers the band energy, in the same way as for the split di-interstitial structures, while the latter pins the excess O $2p$ states at the Fermi level and, as a result, does not allow the same lowering of the band energy. The cubo-octahedron structure shares some of the electronic structure features with the split quadinterstitials, but, as indicated by their higher oxidation energy, these features are not optimized to the same extent for cubo-octahedrons as for split quadinterstitials. We recall that, compared to split di-interstitials, octahedral-interstitial structures benefit from lower Coulomb repulsion among ions. However, unlike the split di-interstitial/octahedral-interstitial energy balance in the low-concentration range (I_2^X vs I_2^S), for the intermediate oxygen concentration range the gain in band energy due to hybridization outweighs the increase in Coulomb repulsion to clearly favor split quadinterstitials over seperated octahedral interstitials (I_4^X vs I_4^S). The oxidation energy of split quadinterstitials is lower than for split di-interstitials, which means that the split quadinterstitial is a bound state of two split di-interstitials (0.70 eV per split quadinterstitial cluster). The high stability for the split quadinterstitial follows from a combination of further increased hybridization and more efficient handling of the repulsive ionic Coulomb contribution from excess O^{2-} ions and charge-compensating U^{5+} ions. Moreover, the binding energy of split quadinterstitials with respect to isolated interstitials in the dilute limit is positive by as much as 0.72 eV per split quadinterstitial.

2. Neptunium and plutonium dioxides

Comparing the results for NpO_{2+x} and PuO_{2+x} with UO_{2+x}, the main conclusion is that the oxidation energies for NpO_{2+x} and PuO_{2+x} are much less negative and, as a result, NpO_2 and PuO_2 should be more difficult to oxidize. PuO_{2+x} is even predicted to have positive oxidation energy, which implies that PuO_2 should not react with O_2, unless another lower energy reaction path is available (discussed in Secs. III C and III D). The observed UO_2, NpO_2, and PuO_2 sequence of increasing oxidation energies correlates with the change in the relative position of the A $5f$ orbitals and the O $2p$ band between UO_2, NpO_2, and PuO_2. The associated decreased gain in O $2p$ band energy compared to the $5f$ delocalization energy explains the high oxidation energy for NpO_{2+x} and PuO_{2+x}. A notable feature for NpO_{2+x} is the very low oxidation energy for I_2^0 compared to other defect clusters, contrasting the properties of UO_{2+x} and PuO_{2+x}. This suggest that optimal bonding in NpO_{2+x} occurs for the I_2^0 geometry, though at present we are unable to explain this particular feature. The stability of split di-interstitials and regular octahedral interstitials is switched between NpO_{2+x} and UO_{2+x}. As discussed in Sec. III C 2 the oxidation energies of PuO_{2+x} are closely related to the ability to avoid unfilled O $2p$ states at the top of the valence band, which, in turn, is related to the degree of hybridization between O $2p/A$ $5f$ orbitals. Increased hybridization removes the unfilled states by occupying empty O $2p$ states and separating the corresponding Pu $5f$ states into either the band gap or to the bottom of the conduction band. Similar, but less pronounced, conclusions hold true for NpO_{2+x}.

Table II also contains the stability of split quadinterstitial clusters and four separated octahedral interstitials in NpO_{2+x} and PuO_{2+x}. The PuO_{2+x} results confirm the trends for UO_{2+x}, in the sense that the split quadinterstitial is predicted to be the most stable state and also bound with respect to I_1 and I_2 structures. The high stability of I_2^0 for NpO_{2+x} shifts the relative stabilities, as compared to UO_{2+x} and PuO_{2+x}, and I_4^X is the second most stable defect structure. Compared to UO_{2+x}, the oxidation energy of split quadinterstitials remains high for both NpO_{2+x} and PuO_{2+x}.

C. Ordering of oxygen clusters in A_4O_9

1. Uranium dioxide

Below 500–1400 K UO_{2+x} phase separates into UO_2 (UO_{2+x}) and ordered U_4O_9 (U_4O_{9-y}).[9,53] The temperature at which the two-phase field transforms into a solid solution is

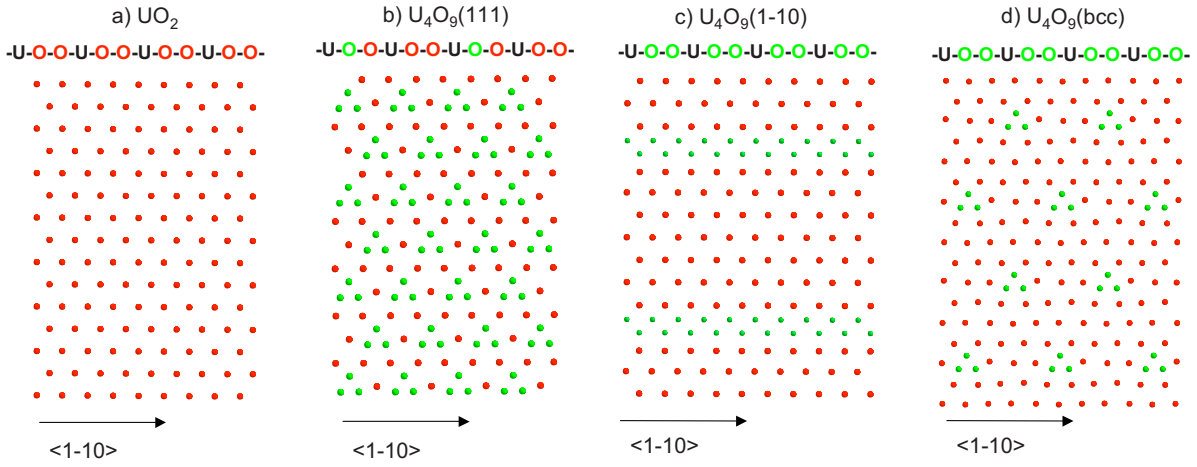

FIG. 5. (Color online) Viewed along the {111} lattice direction, the fluorite lattice is composed of the -U-O-O-U-O-O-U-O-O-U-O-O- sequence of uranium and oxygen planes. This figure demonstrates ordering patterns of split di-interstitials for various U_4O_9 compounds. (a) The hexagonal pattern of oxygen ions in a {111} plane of the UO_2 fluorite lattice. (b), (c), and (d) illustrate the ordering of split di-interstitials (green/light) in {111} planes for (b) $U_4O_9(111)$, (c) $U_4O_9(1-10)$, and (d) U_4O_9(bcc). In the "-U-O-O-U-O-O-U-O-O-U-O-O-" label above figures (a), (b), (c), and (d), the red/dark "O" character symbolizes a regular oxygen plane and the green/light O character symbolizes an oxygen plane that contains excess oxygen ions or defects. Note that this notation does not specify the actual crustallographic periodicity of {111} planes. Red/dark spheres denote regular oxygen ions and green/light spheres represent oxygen ions that are part of the split di-interstitial clusters.

a strong function of composition.[9,53] U_4O_9 is envisioned to be an ordered arrangement of the oxygen defects or clusters in UO_{2+x}. Early neutron-diffraction experiments indicated that U_4O_9 should be described within a $4\times4\times4$ expansion of the conventional fluorite unit cell and Allen *et al.*[54] proposed an ordered arrangement of 2:2:2 clusters along [1 –1 0] lattice vectors. This model was later rejected due to incompatibilities with intensities of neutron-diffraction data.[9,20] The most recent U_4O_9 (U_4O_{9-y}) structure model is an intricate arrangement of the cubo-octahedron type of clusters within the $4\times4\times4$ unit cell.[10] Proceeding from the ground-state configurations of the split di- and quadinterstitials, we now investigate how these may order at the U_4O_9 composition. We first describe the different structure motifs under study, then we discuss their thermodynamic stability, and finally we compare predicted local structure properties with experimental EXAFS measurements.

Two different ordering patterns of split di-interstitials have been considered; split di-interstitials ordered in every fourth {111} plane [$U_4O_9(111)$] and split di-interstitials ordered along [1 –1 0] lattice vectors [$U_4O_9(1-10)$]. $U_4O_9(111)$ is a natural extension of the fact that split di-interstitials occupy {111} planes and $U_4O_9(1-10)$ is inspired by the U_4O_9 structure proposed by Allen *et al.*,[54] but instead of the 2:2:2 cluster, the $U_4O_9(1-10)$ structure uses the split di-interstitial as the expansion unit.

Viewed along the [1 1 1] lattice direction the fluorite lattice is composed of hexagonal U and O layers arranged in a -O-O-U-O-O-U-O-O- sequence; see Fig. 5(a). Figure 5(b) shows the geometry of one of the {111} planes in $U_4O_9(111)$ that contains split di-interstitials. The split di-interstitial oxygen ions are slightly displaced out of the {111} plane, as compared to the regular fluorite oxygen ions in the same {111} plane. The charge-compensating U^{5+} ions in $U_4O_9(111)$ fully occupy the next-nearest-neighbor uranium plane with respect to the split di-interstitials. Sickafus *et al.*[55] discuss how fluorite derived structures such as pyrochlores and various sequioxides can be rationalized in terms of {111} stacking motifs and the $U_4O_9(111)$ structure obviously belongs to this class, though this particular stacking pattern has not been previously identified. Below we outline how all the split di- and quadinterstitial U_4O_9 structures proposed here can be portrayed in terms of {111} stacking motifs based on split di-interstitials.

The starting point for the $U_4O_9(1-10)$ structure is a chain of split di-interstitials separated by the [0.5 –0.5 0] lattice vector. Upon geometry optimization this structure relaxes significantly and the [0.5 –0.5 0] ordering of triangular split di-interstitial motifs transforms into a new stacking pattern, still along [0.5 –0.5 0], but composed of four interstitial-like oxygen ions arranged in a parallelogram. This parallelogram is created from the split di-interstitial by displacing one additional regular oxygen ion from its lattice site, which may also be interpreted as the two excess oxygen ions dislocating two regular oxygen ions, instead of one for the split di-interstitial. This parallelogram is directed along the [0.5 0 0] lattice direction and then stacked with a periodicity of [0.5 –0.5 0], which is prescribed by our choice of unit cell. We note that the adjoining split di-interstitials in the split quad-interstitial cluster also creates a parallelogram (see Fig. 4), which is equivalent to the parallelogram in the $U_4O_9(1-10)$ structure. Thus, $U_4O_9(1-10)$ can be viewed as an interconnected ordering of split quadinterstitials along the [1 –1 0] lattice vector (note that the periodicity is [0.5 –0.5 0]). The U^{5+} ions in the $U_4O_9(1-10)$ structure occupy the four nearest-neighbor positions with respect to the defect oxygen parallelogram. As shown in Fig. 5(c), the $U_4O_9(1-10)$ structure can also be visualized within a {111} stacking model. The cluster ions form chains in the {111} planes and, since the excess ions/defects occupy every {111} plane instead of

every fourth plane as for $U_4O_9(111)$, the concentration of excess ions or defects in each $U_4O_9(1-10)$ {111} plane is 1/4 of the corresponding $U_4O_9(111)$ {111} concentration. Relaxation results in small out of plane shifts within each $U_4O_9(1-10)$ {111} plane.

The split quadinterstitial clusters may also be arranged as separate units within the fluorite lattice and, in principle, arbitrary superstructures of any composition can be created by varying the stacking and orientation of these units. We have investigated two of the most probable configurations within the $2\times2\times2$ supercell; in the first case the split quadinterstitials are ordered along the [1 1 1] vector [U_4O_9(bcc)] and in the second case, one of these split quadinterstitial units is rotated 90° with respect to the other cluster [U_4O_9(bccr)]. Notice that the split quadinterstitials in U_4O_9(bcc) and U_4O_9(bccr) form a bcc lattice, hence the bcc and bccr notation. Even though the true ground-state structure of U_4O_9 may exhibit a longer stacking sequence of split quadinterstitials than allowed within the $2\times2\times2$ cell, we believe that U_4O_9(bcc) and U_4O_9(bccr) serve as appropriate modeling structures, capable of capturing the relevant physics of the U_4O_9 superstructures. Due to the specific geometry of split quadinterstitials, both U_4O_9(bcc) and U_4O_9(bccr) in fact involve stacking of {111} planes that contain an ordered arrangement of split di-interstitials. In these two cases the split di-interstitials occupy every oxygen plane and Fig. 5(d) illustrates the {111} in-plane geometry for U_4O_9(bcc). The {111} planes in U_4O_9(bccr) exhibit the same type of in-plane pattern of split di-interstitials as U_4O_9(bcc), but the stacking sequence differs between the two structures. The split quadinterstitials are made up of two split di-interstitials overlapping between nearest-neighbor {111} planes. There are rather significant out-of-plane distortions for the split di-interstitials in both U_4O_9(bcc) and U_4O_9(bccr).

Following the recipe for U_4O_9(bcc), we have also built U_4O_9 structure models by inserting two cubo-octahedral clusters separated by the [1 1 1] vector in the $2\times2\times2$ cell, labeled U_4O_9(Cubo). These structures represent a simplified version of the $4\times4\times4$ cubo-octahedron structure reported by Bevan *et al.*[9] As reference, we have calculated the stability of U_4O_9 constructed from regular octahedral interstitials [U_4O_9(Oct.)] and undistorted di-interstitials [$U_4O_9(111_0)$].

Table II shows that U_4O_9(bcc) is the most stable U_4O_9 compound, closely followed by U_4O_9(bccr). $U_4O_9(1-10)$ and $U_4O_9(111)$, as well as any structures based on octahedral interstitials, are considerably higher in energy. With reference to Fig. 5 and Table II, we emphasize the stabilizing contribution coming from the covalent bonding (hybridization) in split di-interstitial type of defects and, additionally, the fact that distributing these defects among several planes [compare for example U_4O_9(bcc) and $U_4O_9(111)$] and maximizing the intraplanar separation of split di-interstitials [compare for example U_4O_9(bcc) and $U_4O_9(1-10)$] lowers the contribution from Coulomb repulsion among ions. The stability curve in Fig. 6 demonstrates that the low oxidation energy of single split quadinterstitials (I_4^X) precludes the existence of a pure UO_2-U_4O_9 two-phase field, instead the calculated stability curve suggests the existence of a phase field involving UO_2 and a nonstoichiometric U_4O_{9-y} phase. Our calculations indicate that the rationale for the preference of

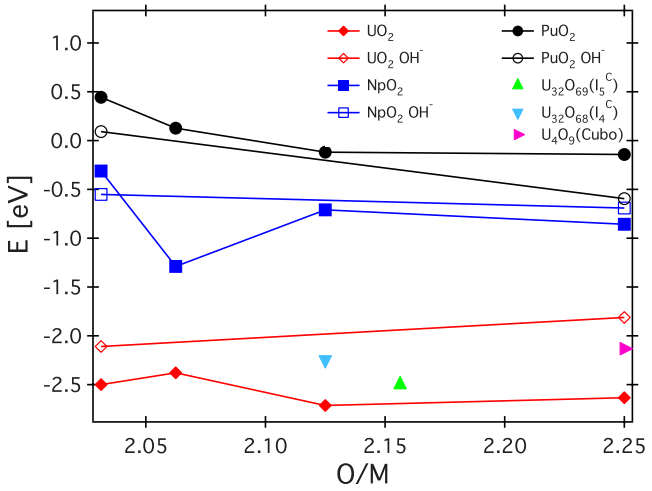

FIG. 6. (Color online) The stability (E) of UO_{2+x}, NpO_{2+x}, and PuO_{2+x}, measured relative to AO_2 and O_2 (oxidation energy). The numbers represent the most stable configuration for each composition. We have also included hydrogen-containing compounds and the cubo-octahedron based UO_{2+x} compounds. In this plot, phase separation would follow if the oxidation energies exhibit negative curvature. Due to the high stability of I_4^X, our calculations do not predict a pure UO_2-U_4O_9 phase equilibrium, but instead they suggest the existence of a $UO_2+U_4O_{9-y}$ phase field.

nonstoichiometric U_4O_{9-y} over stoichiometric U_4O_9 is that oxidation all the way up to U_4O_9 causes frustration among excess oxygen ions and particularly U^{5+} ions, leading to optimal energy balance for the nonstoichiometric phase. In agreement with this reasoning, the experimental phase diagram contains a UO_{2+x}-U_4O_{9-y} phase field rather than UO_{2+x}-U_4O_9.[9,53] The UO_{2+x}-U_4O_{9-y} two-phase field only emerges when the split quadinterstitial type of clusters is taken into account, i.e., I_4^X, U_4O_9(bcc) or U_4O_9(bccr), and this emphasizes the strong influence that clustering or cooperativity has on the UO_{2+x} phase diagram. The U_4O_9 structures based on cubo-octahedron clusters within the $2\times2\times2$ cell are not as stable as U_4O_9(bcc)/U_4O_9(bccr). This contradicts the established experimental U_4O_9 structure models,[9,10] which favors an ordering pattern based on cubo-octahedrons, as an alternative we propose that the low-temperature U_4O_9 compound constitutes an ordered array of split quad-/di-interstitial clusters. We have not been able to investigate U_4O_{9-y} structures based on cubo-octahedron I_5^C clusters, but the more negative oxidation energy of I_4^X compared to I_5^C discussed in Sec. III B emphasizes the importance of the former defect as the fundamental component of U_4O_{9-y} structures.

For $U_4O_9(111)$, U_4O_9(bcc), and U_4O_9(bccr), the {111} in-plane patterns of split di-interstitials are similar to the ordering of triangular oxygen clusters that was obtained by Campbell and Ellis[56] from LEED measurements of the surface structure in oxidized UO_2,[57] thus supporting the pivotal role of the split di- or quadinterstitial as the fundamental building block in UO_{2+x}. Some discrepancies still exist between the structure patterns in Fig. 5 and Refs. 56 and 57, which could be due to thermal disorder, kinetic trapping, or more intricate ordering of split di- or quadinterstitials in the experiments.

The experimental oxidation energy for U_4O_9 is ≈ -1.8 eV,[58] which is notably higher (less negative) than the calculated value of −2.63 eV for U_4O_9(bcc) or −2.71 eV for the split quadinterstitial. This discrepancy may partially be due to uncertainties in the choice of the Hubbard U parameter and/or the exchange-correlation potential. Test calculations using GGA+U with U=3.5 and J=0.35 eV give an oxidation energy of −2.02 eV for U_4O_9(bcc), which agrees better with experiments. The GGA+U UO_2 lattice parameter is overestimated by 0.06 Å and the bulk modulus is predicted to be 194 GPa, in good agreement with experiments (see Table I). The relative stabilities of U_4O_9 compounds within GGA+U are U_4O_9(Oct.) (−0.79 eV), U_4O_9(111) (−1.47 eV), U_4O_9(1−10) (−1.63 eV), U_4O_9(bccr) (−1.94 eV), and U_4O_9(bcc) (−2.02 eV), which is the same stability sequence as obtained for LDA+U and even the stability differences are rather similar [U_4O_9(Oct.) deviates slightly from this conclusion]. Also the balance between U_4O_9(bcc) and the I_4^X cluster, the latter with an oxidation energy of −2.13 eV, is reproduced. From this we conclude that even though the current LDA+U functional overestimates the oxidation energy of UO_{2+x} by 0.8 eV, this shift seems to be rather constant and, most importantly, this implies that the relative defect stabilities, and thus also the proposed oxygen ordering patterns, should be reliable.

In UO_2 there is a single U-O distance of 2.36 Å (for the calculated lattice constant), but oxidation of UO_2 creates a distribution of U-O bond lengths. For U_4O_9(Oct.), the calculations predict the nearest-neighbor U-O bond length to be 2.20 Å and this is largely achieved by displacing the fluorite oxygen ions while the uranium sublattice remains essentially intact. For the split di-interstitial U_4O_9 compounds there is obviously a significant displacement of the oxygen sublattice, but, unlike the U_4O_9(Oct.) compound, there is also an accompanying distortion of the uranium sublattice. Figure 7 illustrates these properties in terms of the uranium radial distribution function for U_4O_9(Oct.) and U_4O_9(bccr). Extended x-ray-absorption fine-structure (EXAFS) measurements by Conradson *et al.*[32] have provided new information about the local structure in UO_{2+x} compounds. Most notably they predict very short oxo type of U-O bonds (1.74 Å).[32] Figure 7 compares the radial distribution function, $g(r)$, from the U_4O_9 structure models that are used in the present work with $g(r)$ derived from EXAFS measurements.[32] Qualitatively, the U_4O_9(bccr) structure model reproduces the broad distribution of U-O bonds between 2.15 and 2.75 Å. The short U-O (2.1−2.2 Å) distances obtained from the structure models proposed here uniquely originate from U^{5+}-O^{2-} distances. The oxo bonds at 1.7−1.8 Å in the EXAFS data are not present in any of the calculated distribution functions, which suggests that the oxo type of bonds should originate from domains, interfaces or surfaces where the regular fluorite structure breaks down.

2. Neptunium and plutonium dioxides

The ordering patterns established above for U_4O_9 have also been applied to the neptunium and plutonium based oxides. The NpO_{2+x} and PuO_{2+x} stabilities are collected in Table II. Np_4O_9 exhibits the same sequence of ordered compounds as U_4O_9, though overall the oxidation energy increases significantly. The Np_4O_9(Oct.) structure is even unstable, though, its stability can be increased considerably (0.76 eV) by allowing half of the octahedral interstitials to form molecular O_2 species with regular fluorite oxygen ions, a process which is further discussed for Pu_4O_9. In conjunction with U_4O_9, Np_4O_9(bcc) is the most stable Np_4O_9 compound followed by Np_4O_9(bccr). As pointed out for NpO_{2+x}, the high oxidation energy for Np_4O_9 compared to U_4O_9 is a consequence of the smaller gain in O 2p band energy relative the A 5f delocalization energy, which in turn follows from the decreased separation of A 5f and O 2p orbitals in NpO_2 compared to UO_2. In order to verify that the decreased stability of Np_4O_9 is principally a band-structure effect and not due to the smaller volume of NpO_2 compared to UO_2, we calculated the NpO_2 oxidation thermodynamics at the UO_2 lattice constant without finding any significant changes. Unlike UO_{2+x} and PuO_{2+x}, the overall most negative NpO_{2+x} oxidation energy occurs for the I_2^0 cluster. The NpO_{2+x} and Np_4O_9 oxidation energies are negative, however, in this context we recall that according to the experimental phase diagram NpO_{2+x} is unstable or possibly metastable with respect to NpO_2+Np_2O_5 (Refs. 13 and 14) or NpO_2+O_2.[4,13,14] According to Ref. 14 the Np_2O_5 oxidation energy is −0.15 eV, which, in relation to our calculated data, implies that Np_4O_9 could exist as a stable compound. However, from U_4O_9 we also know that the LDA+U calculations tend to overestimate the stability of oxidation products. If this overestimation is of the same order of magnitude for Np_4O_9 as for U_4O_9 (0.8 eV), the stability of Np_4O_9 is slightly higher than Np_2O_5. In both cases the oxidation energy is close to 0 eV, implying that disassociation into NpO_2+O_2 should begin even at moderate temperatures and for small changes in the oxygen chemical potential. These conclusions qualitatively agree with the experimental analyses by Neck *at al.*[4] and they are also consis-

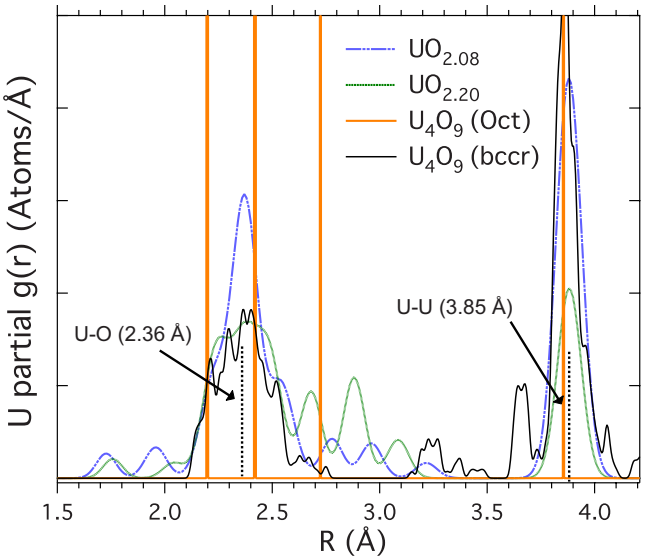

FIG. 7. (Color online) The uranium partial radial distribution function, $g(r)$, calculated from U_4O_9(bccr) and U_4O_9(Oct.) and compared to $g(r)$ from EXAFS measurements on two different UO_{2+x} samples (Ref. 32). The U-O and U-U labels (dotted vertical lines) indicate the bond distances in UO_2.

tent with the difficulty of preparing NpO_{2+x} by direct oxidation of NpO_2,[13] however the low oxidation energy for I_2^0 clusters indicates that partial oxidation of NpO_2 may nevertheless be possible. Moreover, since the oxidation energies of Np_4O_9 and Np_2O_5 are not very different, the fluorite based NpO_{2+x} phase can probably be stabilized by the addition of uranium.

Table II demonstrates that the properties of the Pu_4O_9 compounds are quite different from the corresponding uranium and neptunium compounds. $Pu_4O_9(1-10)$ is the structure of highest energy (this structure is low in energy for U_4O_9 and Np_4O_9) and $Pu_4O_9(111_0)$ is one of the most stable structures (this structure is high in energy for U_4O_9 and Np_4O_9). Pu_4O_9(bcc) is the most stable compound. There is also an octahedral-interstitial structure that is almost as stable as Pu_4O_9(bcc), but this Pu_4O_9 structure includes an O_2 molecular species that is created from an octahedral-interstitial oxygen ion and one of its nearest-neighbor regular fluorite oxygen ions. The O-O bond distance for this molecular species is 1.43 Å. In our calculations, the O_2 species constitute half of the interstitials and the other half acts as regular octahedral interstitials. There is minimal charge transfer from plutonium ions to the O_2 species, which makes it an uncharged molecule rather than an O_2^- or O_2^{2-} ion. The formation of O_2 species lowers the energy by 0.46 eV compared to regular octahedral interstitials. Even for the most stable structures the oxidation energy for Pu_4O_9 is just below zero and PuO_2 should consequently be rather difficult to oxidize, especially if we assume a similar overestimation of the stability of oxidation products as was found for UO_{2+x} [≈0.8 eV per excess oxygen ion]. We have already concluded that the instability of PuO_{2+x} follows from the fact that in PuO_2 the 5*f* orbitals completely overlap with the O 2*p* band, implying that the Pu 5*f* to excess O 2*p* charge transfer does not result in any significant gain in band energy, even if maximum hybridization is assumed. Consequently, charge transfer must be more difficult and this also explains why the excess oxygen ions are not able to attract two full electrons from the plutonium ions, or more precisely attain the O^{2-} valence state (see Sec. III A). Analogous arguments partially hold for NpO_{2+x}, but since the Np 5*f* states are situated at the top of the O 2*p* band charge transfer is still easier than for PuO_{2+x}. The incomplete charge transfer in PuO_{2+x} (and NpO_{2+x}) creates unfilled states in the O 2*p* valence band (see Fig. 8), which from a chemical point of view, is unfavorable. The formation of O_2 species within the lattice in part removes the unfilled O 2*p* states and separates the remaining states from the valence band, thus explaining the increased stability for this compound. The most stable Pu_4O_9(bcc) compound exhibits a high degree of hybridization and thus also yields high plutonium to excess oxygen charge transfer (i.e., valence states close to Pu^{5+} and O^{2-}). Increased hybridization yields largely filled O 2*p* states for Pu_4O_9(bcc) and, correspondingly, the now empty Pu 5*f* states either move into the band gap or attaches to the lower part of the conduction band. Our calculations show that the relative stabilities of PuO_{2+x} structures are correlated with the ability to increase O 2*p* hybridization and thus avoid unfilled O 2*p* states at the top of the valence band, which introduces a rather high sensitivity to structural details, in particular for defect configurations that exhibit high oxidation energy. This conclusion is similar to the observation that the energy of Pu_4O_9(Oct.) decreases by displacing the octahedral interstitial from its high-symmetry position made by Prodan *et al.*[21]

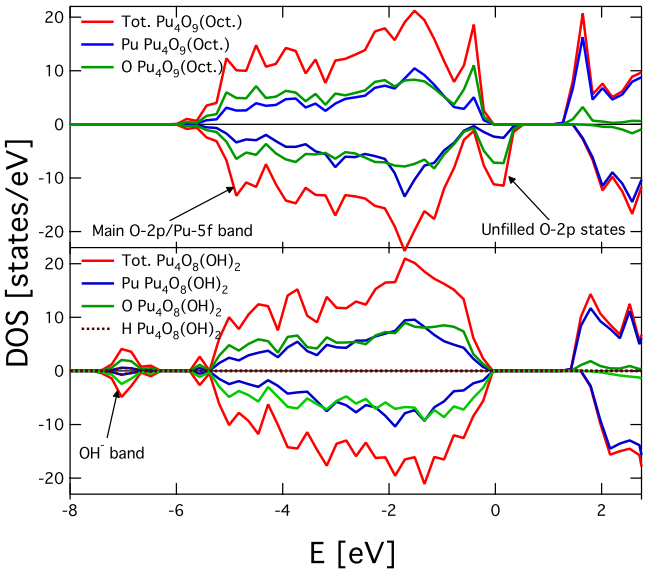

FIG. 8. (Color online) Density of states and projected density of states for Pu_4O_9(Oct.) and $Pu_4O_8(OH)_2$. For the Pu_4O_9(Oct.) structure we observe the unfilled O 2*p* states at the top of the valence band. By introducing distortions to the octahedral Pu_4O_9 structure, the unfilled O 2*p* states may become occupied due to increased hybridization and instead the emptied Pu 5*f* states are transferred into either the band gap or the bottom conduction band, which is a process that lowers the energy. The unoccupied O 2*p* states at the top of the valence band disappear for $Pu_4O_8(OH)_2$ and instead the OH^- band appears below the main O 2*p* band. The highest occupied state is at 0 eV.

D. Hydrogen affinity of AO_{2+x} and A_4O_9

The PuO_2 oxidation thermodynamics presented in Secs. III B 2 and III C 2 partially contradict the findings by Haschke and co-workers,[6,7] who claimed to be able to oxidize PuO_{2+x} up to $x=0.27$. On the other hand our results support failures to produce bulk PuO_{2+x} from PuO_2 by using pure oxygen as oxidation agent.[59] The fact that Haschke *et al.* used moist air as oxidation agent and the fact that Conradson *et al.*[12] found PuO_{2+x} to readily incorporate H_2O or its radiolysis products (e.g., OH^-) in the lattice point to the critical role of these species in the oxidation process. Based on analogies to UO_{2+x}, Neck *et al.*[4] further emphasized the importance of H_2O by estimating anhydrous PuO_{2+x} to be unstable, which disagrees with the oxidation mechanism proposed by Haschke and co-workers.[6,7] Their estimated Pu_4O_9 oxidation energy of 0.13 eV (Ref. 4) is higher than the present calculations (−0.14 eV), though from U_4O_9 we know that the LDA+*U* calculations have a tendency to overestimate oxidation energies. Assuming the Pu_4O_9 error to be similar to U_4O_9, e.g., 0.8 eV, we predict even more positive oxidation energies than Neck *et al.*,[4] thus emphasizing the endothermic character of this reaction. On the other hand

Neck *et al.* predicted hydrous Pu_4O_9 (Pu_4O_9 associated with H_2O) to have slightly negative oxidation energy (−0.12 eV).[4]

These observations motivate us to study oxidation thermodynamics based on absorption of OH^- or H_2O in the AO_2 lattice. This was achieved by inserting hydrogen atoms into the $2\times2\times2$ supercell that contains single oxygen interstitial. The hydrogen atoms prefer to bind to the oxygen ion in the octahedral-interstitial position and align themselves in the [1 1 1] directions, which means that they are situated in between two oxygen ions but the distance to the octahedral oxygen ion is shorter than to the regular fluorite ion. In the case of H_2O the two hydrogen atoms form an approximately 180° angle with the interstitial oxygen ion. Using similar procedures as for the $2\times2\times2$ cell we have also studied $A_4O_8(OH)_2$ within the same cell as was used for $A_4O_9(111)$. The oxidation energies are summarized in Table II and they are also illustrated in Fig. 6. For PuO_{2+x} the presence of OH^- species lowers the oxidation energy significantly, in particular for $Pu_4O_8(OH)_2$, so that oxidation of PuO_2 becomes a more exothermic reaction. Measured against oxidation based on OH^- species, absorption of H_2O species is less likely to occur; as an example the oxidation energy of $PuO_2(H_2O)_{1/32}$ is 0.47 eV.

Our results suggest that oxidation of PuO_2 requires the presence of H_2O in order to take place at any significant rate. This would explain why Gouder *et al.*[59] failed to oxidize PuO_2 using pure oxygen as oxidation agent, while Haschke *et al.* observed oxidation in moist air. The lattice constant of $Pu_4O_8(OH)_2$ exhibits a small expansion, which agrees with the experimental observation by Haschke *et al.*[6] In this context we observe that $U_4O_9(1-10)$ and $Np_4O_9(1-10)$ both contract by 0.01–0.02 Å. Experimentally, U_4O_9 contracts by 0.03 Å, measured as an average for the $4\times4\times4$ unit cell.[9] The reason for $Pu_4O_8(OH)_2$ being the most stable oxidation product of PuO_2 lies in the change of the band structure induced by hydrogen. Figure 8 illustrates how the orbitals of the OH^- species are situated about 0.50 eV below the main O $2p$ band, which implies that the electron transferred from plutonium to the OH^- species moves down from the hybridized O $2p$–Pu $5f$ band to the OH band and this results in a gain in the band energy, much like the process for split di-interstitials in UO_{2+x}. Also, the electron donated by hydrogen means that only one plutonium electron needs to be transferred to achieve filled O $2p$ orbitals. The negative oxidation energy of $Pu_4O_8(OH)_2$ is consistent with the oxidation energy of −0.12 eV predicted by Neck *et al.*[9] for hydrous PuO_2. Our experience from U_4O_9 tell us that we slightly overestimate the stability of oxidation products and, consequently, we expect the oxidation energy of $Pu_4O_8(OH)_2$ to increase (become less negative), however even if the upper limit of the error for U_4O_9 is applied as correction (0.8 eV) the oxidation energy of $Pu_4O_8(OH)_2$ is at least close to zero and may thus be thermodynamically allowed. In any case, $Pu_4O_8(OH)_2$ is more stable than the corresponding hydrogen-free compounds.

Even though the $UO_2(OH)_{1/32}$ and $U_4O_8(OH)_2$ compounds have negative oxidation energies, both are less stable than the corresponding pure oxides and thus they release any absorbed hydrogen, which agrees with established oxidation thermodynamics of UO_2.[3] $U_4O_8(OH)_2$ exhibits a similar OH^- band below the main O $2p$ band as $Pu_4O_8(OH)_2$. The fact that UO_{2+x} does not attract hydrogen means that the contribution from decreased band energy due to O $2p$ hybridization is more important. Notice that $U_4O_8(OH)_2$ is indeed more stable than the U_4O_9(Oct.) structure, for which hybridization effects are small compared to the most stable U_4O_9 compounds. The $Np_4O_8(OH)_2$ compound is somewhat higher in energy than Np_4O_9(bcc).

IV. CONCLUSIONS

The excess oxygen ions in hyperstoichiometric actinide dioxides, AO_{2+x} (A=U, Np, or Pu), form clusters of interstitial oxygen ions and, using density functional theory calculations, we have established the so-called split di-interstitial, illustrated in Fig. 1, as the fundamental building block of these defect clusters. The most stable configuration constitutes two split di-interstitials that are rotated 180° with respect to each other, as illustrated in Fig. 4. Our calculations demonstrate that the stability of these clusters is an effect of the increased hybridization between actinide ions and excess oxygen ions. We also predict a new ground-state structure for U_4O_9 that is based on a superstructure of split quadinterstitials, which, alternatively, can be visualized as a stacking of {111} planes that contain an ordered arrangement of split di-interstitials.

The structural insights acquired from the present density functional theory calculations allow us to accurately assess the oxidation thermodynamics of UO_2, NpO_2, and PuO_2 within fluorite derived structures. UO_2 exhibits strongly negative oxidation energy and reacts readily with oxygen, while NpO_2 is significantly harder to oxidize and PuO_2 is predicted to have positive, or just slightly negative, oxidation energy. The degree of AO_2 oxidation is a function of the position of the A $5f$ electrons relative the O $2p$ band. If these states are situated above the O $2p$ band, oxidation easily occurs (UO_2), while the overlap of A $5f$ and O $2p$ states in PuO_2 suppresses oxidation. The presence of H_2O and hydrolysis products is able to offset this effect and turn oxidation of PuO_2 into an exothermic process.

ACKNOWLEDGMENTS

Work at Los Alamos National Laboratory was funded by the Global Nuclear Energy Partnership Fuels Campaign, and OBES Division of Chemical Sciences under contract W-7405. D.A.A. also acknowledges support from the Seaborg Institiute at Los Alamos National Laboratory. Los Alamos National Laboratory is operated by Los Alamos National Security, LLC, for the National Nuclear Security Administration of the U.S. DOE under Contract No. DE-AC52-06NA25396. C.D. was supported by DOE NERI-C Grant No. DEFG07-14891.

[1] L. R. Morss, in *The Chemistry of the Actinide Elements*, 2nd ed., edited by J. J. Katz, G. T. Seaborg, and L. R. Morss (Chapman and Hall, London, 1986), Vol. 2.
[2] M. W. Chase, *JANAF Thermochemical Tables*, 3rd ed. (AIP, New York, 1985).
[3] I. Barin, O. Knacke, and O. Kubaschewski, *Thermochemical Properties of Inorganic Substances* (Springer, Berlin, 1977).
[4] V. Neck, M. Altmaier, and Th. Fanghänel, J. Alloys Compd. **444-445**, 464 (2007).
[5] C. Keller, in *Comprehensive Inorganic Chemistry*, edited by J. C. Bailar, H. J. Emeleus, R. Nyholm, and A. F. Trotman-Dickenson (Pergamon, Oxford, 1973) Vol. 5.
[6] J. M. Haschke, T. H. Allen, and L. A. Morales, Science **287**, 285 (2000).
[7] J. M. Haschke and T. H. Allen, J. Alloys Compd. **336**, 124 (2002).
[8] P. Martin, S. Grandjean, M. Ripert, M. Freyss, P. Blanc, and T. Petit, J. Nucl. Mater. **320**, 138 (2003).
[9] D. J. M. Bevan, I. E. Grey, and B. T. M. Willis, J. Solid State Chem. **61**, 1 (1986).
[10] R. I. Cooper and B. T. M. Willis, Acta Crystallogr., Sect. A: Found. Crystallogr. **60**, 322 (2004).
[11] S. D. Conradson, B. D. Begg, D. L. Clark, C. Den Auwer, F. J. Espinosa-Faller, P. L. Gordon, N. J. Hess, R. Hess, D. W. Keogh, L. A. Morales, M. P. Neu, W. Runde, C. D. Tait, D. K. Veirs, and P. M. Villella, Inorg. Chem. **42**, 3715 (2003).
[12] S. D. Conradson, B. D. Begg, D. L. Clark, C. den Auwer, M. Ding, P. K. Dorhout, F. J. Espinosa-Faller, P. L. Gordon, R. G. Haire, and N. J. Hess, J. Am. Chem. Soc. **126**, 13443 (2004).
[13] K. Richter and C. Sari, J. Nucl. Mater. **148**, 266 (1987).
[14] *Chemical Thermodynamics of Neptunium and Plutonium*, edited by R. J. Lemire, J. Fuger, H. Nitsche, P. Potter, M. H. Rand, J. Rydberg, K. Spahiu, J. C. Sullivan, W. J. Ullman, P. Vitorge, and H. Wanner (North-Holland, Amsterdam, 2001), Vol. 4.
[15] M. Freyss, T. Petit, and J.-P. Crocombette, J. Nucl. Mater. **347**, 44 (2005).
[16] P. A. Korzhavyi, L. Vitos, D. A. Andersson, and B. Johansson, Nature Mater. **3**, 225 (2004).
[17] J. P. Crocombette, F. Jollet, T. N. Le, and T. Petit, Phys. Rev. B **64**, 104107 (2001).
[18] M. Iwasawa, Y. Chen, Y. Kaneta, T. Ohnuma, H. Y. Geng, and M. Kinoshita, Mater. Trans. **47**, 2651 (2006).
[19] F. Gupta, G. Brillant, and A. Pasturel, Philos. Mag. **87**, 2561 (2007).
[20] H. Y. Geng, Y. Chen, Y. Kaneta, M. Iwasawa, T. Ohnuma, and M. Kinoshita, Phys. Rev. B **77**, 104120 (2008).
[21] I. D. Prodan, G. E. Scuseria, J. A. Sordo, K. N. Kudin, and R. L. Martin, J. Chem. Phys. **123**, 014703 (2005).
[22] L. Petit, A. Svane, Z. Szotek, and W. M. Temmerman, Science **301**, 498 (2003).
[23] S. L. Dudarev, D. N. Manh, and A. P. Sutton, Philos. Mag. B **75**, 613 (1997).
[24] B. Sun, P. Zhang, and X.-G. Zhao, J. Chem. Phys. **128**, 084705 (2008).
[25] S. Bo and P. Zhang, Chin. Phys. B **17**, 1364 (2008).
[26] G. Jomard, B. Amadon, F. Bottin, and M. Torrent, Phys. Rev. B **78**, 075125 (2008).
[27] R. Laskowski, G. K. H. Madsen, P. Blaha and K. Schwarz, Phys. Rev. B **69**, 140408(R) (2004).
[28] I. D. Prodan, G. E. Scuseria, and R. L. Martin, Phys. Rev. B **76**, 033101 (2007).
[29] K. N. Kudin, G. E. Scuseria, and R. L. Martin, Phys. Rev. Lett. **89**, 266402 (2002).
[30] I. D. Prodan, G. E. Scuseria, and R. L. Martin, Phys. Rev. B **73**, 045104 (2006).
[31] Q. Yin and S. Y. Savrasov, Phys. Rev. Lett. **100**, 225504 (2008).
[32] S. D. Conradson, D. Manara, F. Wastin, D. L. Clark, G. H. Lander, L. A. Morales, J. Rebizant, and V. V. Rondinella, Inorg. Chem. **43**, 6922 (2004).
[33] B. T. M. Willis, J. Chem. Soc., Faraday Trans. 2 **83**, 1073 (1987).
[34] B. T. M. Willis, Proc. Br. Ceram. Soc. **1**, 9 (1974).
[35] B. T. M. Willis, Acta Crystallogr., Sect. A: Cryst. Phys., Diffr., Theor. Gen. Crystallogr. **34**, 88 (1978).
[36] B. T. M. Willis, Nature (London) **197**, 755 (1963).
[37] H. Y. Geng, Y. Chen, Y. Kaneta and M. Kinoshita, Phys. Rev. B **77**, 180101(R) (2008).
[38] G. Kresse and J. Hafner, Phys. Rev. B **48**, 13115 (1993).
[39] G. Kresse and J. Furthmüller, Comput. Mater. Sci. **6**, 15 (1996).
[40] G. Kresse and J. Furthmüller, Phys. Rev. B **54**, 11169 (1996).
[41] G. Kresse and D. Joubert, Phys. Rev. B **59**, 1758 (1999).
[42] P. E. Blöchl, Phys. Rev. B **50**, 17953 (1994).
[43] A. I. Liechtenstein, V. I. Anisimov, and J. Zaanen, Phys. Rev. B **52**, R5467 (1995).
[44] T. Yamashita, N. Nitani, T. Tsuji, and H. Inagaki, J. Nucl. Mater. **247**, 90 (1997).
[45] U. Benedict, S. Dabos, C. Dufour, and J. C. Spirlet, J. Less Common Met. **121**, 461 (1986).
[46] M. Idiri, T. Le Bihan, S. Heathman, and J. Rebizant, Phys. Rev. B **70**, 014113 (2004).
[47] H. J. Monkhorst and J. D. Pack, Phys. Rev. B **13**, 5188 (1976).
[48] S. Kurth, J. P. Perdew, and P. Blaha, Int. J. Quantum Chem. **75**, 889 (1999).
[49] D. A. Andersson, S. I. Simak, B. Johansson, I. A. Abrikosov, and N. V. Skorodumova, Phys. Rev. B **75**, 035109 (2007).
[50] T. Ichinomiya, B. P. Uberuaga, K. Sickafus, Y. Nishiura, M. Itakura, Y. Chen, Y. Keneta, and M. Kinoshita, J. Nucl. Mater (to be published).
[51] K. Govers, S. Lemehov, M. Hou, and M. Verwerft, J. Nucl. Mater. **366**, 161 (2007).
[52] D. A. Andersson, C. Deo and B. P. Uberuaga (unpublished).
[53] Y. Soo Kim, J. Nucl. Mater. **279**, 173 (2000).
[54] G. C. Allen, P. A. Tempest, and J. W. Tyler, Nature (London) **295**, 48 (1982).
[55] K. Sickafus, R. W. Grimes, S. M. Corish, A. R. Cleave, M. Tang, C. R. Stanek, B. P. Uberuaga, and J. A. Valdez, Los Alamos-Series Report No. LA-14205, 2006 (unpublished).
[56] B. D. Campbell and W. P. Ellis, Surf. Sci. **10**, 124 (1968).
[57] G. C. Allen and P. A. Tempest, Proc. R. Soc. London, Ser. A **406**, 325 (1986).
[58] P.-Y. Chevalier, E. Fisher, and B. Cheynet, J. Nucl. Mater. **303**, 1 (2002).
[59] T. Gouder, A. Seibert, L. Havela, and J. Rebizant, Surf. Sci. **601**, L77 (2007).